

Effect of calcium and potassium oxide addition on the viscosity and fragility of a calcium aluminosilicate melt

Sukenaga, Sohei

Institute of Multidisciplinary Research for Advanced Materials, Tohoku University

Gueguen, Yann

Univ Rennes, CNRS, IPR (Institut de Physique de Rennes)

Celarie, Fabrice

Univ Rennes, CNRS, IPR (Institut de Physique de Rennes)

Rouxel, Tanguy

Univ Rennes, CNRS, IPR (Institut de Physique de Rennes)

他


<https://hdl.handle.net/2324/7323625>

出版情報 : Journal of the American Ceramic Society. 107 (6), pp.3822-3836, 2024-01-31. Wiley
バージョン :
権利関係 : © 2024 The Authors.



RESEARCH ARTICLE

Effect of calcium and potassium oxide addition on the viscosity and fragility of a calcium aluminosilicate melt

Sohei Sukenaga¹  | Yann Gueguen²  | Fabrice Celarie² | Tanguy Rouxel² |
 Masanori Tashiro¹ | Shinichiro Yoshida³ | Noritaka Saito⁴ |
 Kunihiro Nakashima⁴ | Hiroyuki Shibata¹

¹Institute of Multidisciplinary Research for Advanced Materials, Tohoku University, Sendai, Japan

²Univ Rennes, CNRS, IPR (Institut de Physique de Rennes) - UMR 6251, Rennes, France

³Research and Analytical Center for Giant Molecules, Tohoku University, Sendai, Japan

⁴Department of Materials, Kyushu University, Fukuoka, Japan

Correspondence

Sohei Sukenaga, Institute of Multidisciplinary Research for Advanced Materials, Tohoku University, Aoba-ku, Sendai 9808577, Japan.
 Email: sohei.sukenaga.d3@tohoku.ac.jp

Funding information

Ministry of Education, Culture, Sports, Science, and Technology of Japan; Institute of Multidisciplinary Research for Advanced Materials, Tohoku University 2014-2015, 2023; Japan Society for the Promotion of Science, Grant/Award Number: JP21H01854

Abstract

Fragility is commonly quantified as the magnitude of change in viscosity at a temperature close to the glass transition temperature (T_g). It is a critical characteristic of melts used in scientific and industrial applications. The fragility of silicate melts generally increases with the depolymerization of silicate anions upon the addition of alkali or alkaline earth oxides. However, the effects of oxide additives on the fragility of aluminosilicate melts remain unclear. In this study, the effect of CaO or K₂O addition on the viscosity of the 36CaO–51SiO₂–13Al₂O₃ (mol.%) melt for the wide viscosity range of 10^{–1}–10¹² Pa s was studied. The relationship between the logarithmic viscosity and T_g -scaled temperature indicated that the melt fragility increased with the addition of CaO, whereas the addition of K₂O reduced the fragility when the additive content of CaO or K₂O was less than 10.8 mol.%. The effect of the addition of K₂O on fragility cannot be explained by the depolymerization of silicate anions alone. Raman and ²⁷Al nuclear magnetic resonance spectroscopies of the glasses indicated that a decrease in the level of distortion of the AlO₄ tetrahedra decreased the fragility of the aluminosilicate melt.

KEYWORDS

aluminosilicate glass, aluminosilicate melt, fragility, viscosity

1 | INTRODUCTION

The viscosities of liquids increase with decreasing temperature and should be ~10¹² Pa s at their glass transition temperatures (T_g), which are reference temperatures for glass-forming systems. Previous studies¹ attempted to determine characteristics of liquids based on the temperature dependences of their viscosities (η), which are

commonly expressed using Arrhenius-type Equation (1) in the narrow temperature range at $\sim T_g$:

$$\log \eta = Y + \frac{E_g}{2.303 \cdot R \cdot T} \quad (1)$$

where Y is a composition-dependent constant, R ($= 8.314 \text{ J mol}^{-1} \text{ K}^{-1}$) is the gas constant, and T is the absolute

This is an open access article under the terms of the [Creative Commons Attribution-NonCommercial](https://creativecommons.org/licenses/by-nc/4.0/) License, which permits use, distribution and reproduction in any medium, provided the original work is properly cited and is not used for commercial purposes.

© 2024 The Authors. *Journal of the American Ceramic Society* published by Wiley Periodicals LLC on behalf of American Ceramic Society.

temperature. In principle, the apparent activation energy (E_g) in Equation (1) can be obtained from the temperature dependence of the η . Nevertheless, for the most part, as E_g depends on T , it spreads over a relatively large range in the case of noncrystalline materials, that is, it decreases with an increase of T .^{2,3,4} Angel^{5,6} quantified the slope of the T_g -scaled Arrhenius plot of viscosity at temperatures of $\sim T_g$, that is, the fragility index m , which is derived using the following equation^{7–11}:

$$m = \frac{E_g}{2.303 \cdot R \cdot T_g} \quad (2)$$

where m is used as an indicator to categorize liquids: (i) strong systems that exhibit modest changes in viscosity with temperature and (ii) fragile liquids that display drastic changes in viscosity at temperatures of $\sim T_g$. Understanding the factors controlling fragility is of significant interest to glass science researchers. In industrial glass-making processes, fragility is used as a measure of glass-forming ability, and the working temperature range in which the viscosity is 10^3 – 10^4 Pa s^{12,13} is appropriate for glass shaping. Generally, shaping a strong system is simpler than shaping a fragile system; thus, the compositional dependence of fragility has been studied for industrial applications, particularly alkali silicate systems. Previous studies^{14–17} have reported that the fragilities of silicate melts increase with the depolymerization of silicate anions upon the addition of metal oxides (e.g., alkali oxides) when the number of nonbridging O atoms per tetrahedrally coordinated cation (NBO/T) is <2 (an example is shown in Figure 1). However, the effects of alkali oxides on the fragility of complex aluminosilicate systems remain unclear. Alkali and alkaline earth cations (i.e., non-framework cations) exhibit alternative structural roles depending on their composition and may function as network modifiers or charge compensators. When Al cations occur as AlO_4 tetrahedra in silicate anions, the bridging O (BO) atoms between the Si and Al cations (i.e., $\text{Si-O}_{\text{BO}}\text{-Al}$) display residual negative charges of $-1/4$ because O exhibits a formal charge of -2 and the respective contributions of the tetracoordinated Si and Al cations are $+1$ and $+3/4$. Non-framework cations (e.g., Ca^{2+}) are required to balance the negative charges of $-1/4$ around the $\text{Si-O}_{\text{BO}}\text{-Al}$ species.^{18,19} The positive charges of these non-framework cations are preferentially used to balance the negative charge of $\text{Si-O}_{\text{BO}}\text{-Al}$, and the excess non-framework cations then act as network modifiers.²⁰ Therefore, the aluminosilicate systems are categorized into three types, depending on the $(\text{RO} + \text{R}_2\text{O})/\text{Al}_2\text{O}_3$ molar ratio, where R represents the alkaline earth or alkali element: peralkaline $((\text{RO} + \text{R}_2\text{O})/\text{Al}_2\text{O}_3 > 1)$, meta-aluminous $((\text{RO} + \text{R}_2\text{O})/\text{Al}_2\text{O}_3 = 1)$, and peraluminous $((\text{RO} + \text{R}_2\text{O})/\text{Al}_2\text{O}_3 < 1)$.²⁰ In the peralkaline and meta-

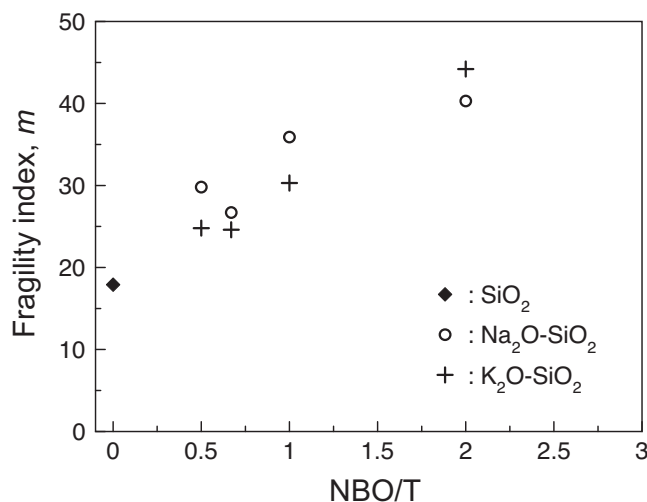


FIGURE 1 Fragility index m of binary alkali silicate melts reported by Nascimento and Aparicio¹⁷ plotted against NBO/T. They fit the viscosity data, which were measured by numerous researchers, using the Vogel–Fulcher–Tammann (VFT) model (see Equation 6). $m (= BT_g/(T_g - C)^2)$ was determined from the fitting parameters of the VFT model. NBO/T is calculated from the nominal compositions.

aluminous composition, aluminum cations tend to form AlO_4 tetrahedra because sufficient charge compensators neutralize the negative charge near $\text{Si-O}_{\text{BO}}\text{-Al}$, whereas the five- or six- coordinated aluminum is easily formed in the peraluminous region where aluminum cations lack the charge compensator.²⁰ Most non-framework cations act as charge compensators in meta-aluminous compositions, whereas excess non-framework cations act as modifiers, which form NBOs on SiO_4 tetrahedra in peralkaline compositions. In peralkaline aluminosilicate melts containing more than two types of non-framework cations, the preferential roles of these cations depend strongly on their average bond valences. These values are expressed as the ratios of the valence numbers (Z) to the coordination numbers (N) of the cations, that is, Z/N .²¹ As the negative charges of $-1/4$ on the $\text{Si-O}_{\text{BO}}\text{-Al}$ BO atoms are smaller than that of Si-O_{NBO} (-1), cations with lower bond valences generally act as compensators, whereas those with higher bond valences preferentially bond with Si-O_{NBO} in SiO_4 tetrahedra.^{18,22,23} Among the aluminosilicate glasses, $\text{CaO-SiO}_2\text{-Al}_2\text{O}_3$ is one of the most critical systems for industrial glasses and melts, and alkali oxides (e.g., Na_2O and K_2O) have been used as additives to control their properties. Assuming that N values of common alkali cations (i.e., Li, Na, and K) are 4 (Li),²⁴ 6 (Na),²⁴ and 7 (K),²⁴ the estimated Z/N values of these cations are 0.25 (Li), 0.17 (Na), and 0.14 (K), where the Z/N of Ca cations should be close to 0.28 assuming N is 7,^{19,25} the estimated Z/N indicates that K cations should have the strongest preference

among these alkali cations to act as compensators of Si-O_{BO}-Al BO atoms in the calcium aluminosilicate systems. Thus, adding K₂O to the peralkaline CaO-SiO₂-Al₂O₃ system may result in two structural changes: (i) an increase in the depolymerization of the silicate anions and (ii) partial substitution of the Ca cations as charge compensators with K cations at Si-O_{BO}-Al. These potential structural changes are consistent with previous structural analyses using ¹⁷O nuclear magnetic resonance (NMR) spectroscopy,^{26,27} and the former should increase fragility, as shown in Figure 1. In terms of the effect of the latter structural change on fragility, in meta-aluminous compositions, alkali aluminosilicate melts exhibit lower fragilities than those of alkaline earth aluminosilicate melts.^{28,29} Although their detailed mechanisms remain unclear, the latter structural change should display contrasting effects on fragility compared to those of the former: The former should increase fragility, whereas the latter should decrease fragility. Therefore, estimating the change in the fragility of the CaO-SiO₂-Al₂O₃ system caused by the addition of K₂O remains challenging, and the change should differ when CaO is added, which simply increases the NBO content of the system. Further experimental studies are required to elucidate these changes in fragility. In our previous study,²⁶ we measured the viscosity of CaO-SiO₂-Al₂O₃ melt by adding K₂O at temperatures higher than 1673 K and found that the viscosity increased with increasing K₂O content. However, the mechanism underlying the increase in viscosity remains unclear. In addition, the viscosity of the lower-temperature region was not investigated, and the impact of K₂O addition on the fragility of the CaO-SiO₂-Al₂O₃ system has not been evaluated. This study investigated the effect of K₂O or CaO addition on the viscosity of a peralkaline CaO-SiO₂-Al₂O₃ melt with NBO/T < 1, which is in the range of the composition of industrial glass materials (e.g., display glass), for a viscosity range wide enough to derive fragility. The changes in the viscosity and fragility observed upon the addition of K₂O were compared with those observed upon the addition of CaO.

2 | EXPERIMENTAL PROCEDURES

2.1 | Samples

The chemical compositions of the samples used for the viscosity measurements are listed in Table 1. In this study, 36 mol.% CaO–51 mol.% SiO₂–13 mol.% Al₂O₃ (CAS), which exhibits a nominal NBO/T of 0.6, was used as the parent composition. The nominal NBO/T ($= (2X_O - 4X_T)/X_T$)³⁰ was derived from the composition, where X_O and X_T are the respective atomic fractions of the O and the fourfold coordinated species (i.e., T = Si

TABLE 1 Nominal and analyzed compositions (mol.%) and NBO/T of the samples.

Samples		Composition (mol.%)				
		CaO	SiO ₂	Al ₂ O ₃	K ₂ O	NBO/T ^a
CAS	nom.	36.0	51.0	13.0	-	0.60
	obs.	36.9	50.2	12.9	-	0.63
CAS + 7.7K	nom.	32.8	46.5	13.0	7.7	0.76
	obs.	33.2	45.9	13.0	7.9	0.78
CAS + 10.8K	nom.	31.6	44.6	13.0	10.8	0.83
	obs.	32.2	43.9	13.1	10.8	0.85
CAS + 7.7Ca	nom.	40.5	46.5	13.0	-	0.76
	obs.	41.3	45.7	13.0	-	0.79
CAS + 10.8Ca	nom.	42.4	44.6	13.0	-	0.83
	obs.	43.1	43.7	13.2	-	0.85

^aNominal NBO/T ($= (2X_O - 4X_T)/X_T$) is derived from the composition, where X_O and X_T are the respective atomic fractions of the O and T species (i.e., Si and Al).

and Al). Because the chosen compositions were in the peralkaline region, we assumed that all Al cations form AlO₄ tetrahedra in the glass in this calculation. The additive effect of K₂O was compared with that of CaO when the Al₂O₃ content remained constant. The K₂O- and CaO-doped samples are, respectively, denoted CAS + xK and CAS + xCa where x represents the molar content of K₂O or CaO. Reagent powders of CaCO₃ (FUJIFILM Wako Pure Chemical Corporation), SiO₂ (FUJIFILM Wako Pure Chemical Corporation), Al₂O₃ (Sigma-Aldrich Co. LLC), and K₂CO₃ (Sigma-Aldrich Co. LLC) were carefully weighed and mixed using a mullite mortar and pestle. The powder mixture was placed in a 30 mL platinum crucible and melted at 1853 K for 15 min. After melting, the samples were quenched on a copper plate to obtain glassy samples. The quenched samples were used for viscosity measurements in high-temperature regions using the rotating cylinder method. For clarity, these compositions are plotted in the (CaO+K₂O)-SiO₂-Al₂O₃ pseudo-ternary diagram shown in Figure 2.

2.2 | Viscosity measurement in low-viscosity region

Viscosity measurements over a wide temperature range T_g –1873 K are required to determine the characteristics of melts based on their viscosities. In this temperature range, as the viscosity of the melt varies significantly from 0.1 to 10¹² Pa s, these changes cannot be measured using a single measurement technique.³¹ To cover the wide range of viscosity variation, the present study used rotating cylinder, parallel plate methods as well as differential thermal

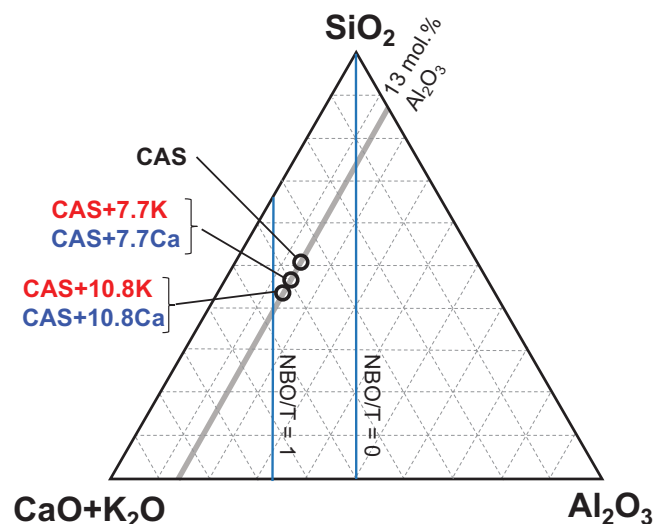


FIGURE 2 Compositions of the samples plotted in a (CaO+K₂O)–SiO₂–Al₂O₃ pseudo-ternary diagram. The gray solid line indicates the molar content of Al₂O₃ of 13 mol.%, and the blue solid lines represent the compositions with NBO/T = 1 and 0. (Color online).

analysis (DTA). The viscosities of the sample melts in the viscosity range of 10^{−1}–10 Pa s were measured using the rotating cylinder method. Detailed information on the rotating crucible-type viscometer is provided in our previous reports.³² The quenched samples (~40 g) were placed in a Pt-20mass%Rh crucible (inner diameter: 30 mm and height: 27 mm) and heated to 1823 K in air. A bob (diameter: 15 mm and height: 8 mm) composed of a Pt-20mass%Rh alloy was immersed in the melt to an immersion depth of 10 mm. The samples were melted for 60 min at 1823 K to ensure compositional and temperature homogeneities. After melting, the viscosity was measured at a crucible rotation rate of 60 rpm during the cooling process in the temperature range of 1823–1673 K in 25 K increments. At each temperature, the samples were melted for more than 15 min to ensure the temperature homogeneity of the melt. The torque exerted on the bob was measured four times. The averaged value was used to determine the viscosities at the given temperatures. The repetitive errors in the measurements were less than 1.5%. After the measurements, the samples were reheated to 1823 K and cast in a graphite mold. The obtained bulk glass was annealed for more than 10 h at temperatures close to the glass transition temperature. The annealed glass samples were used for viscosity measurements in the high-viscosity (lower temperature) region as well as for measurements of the glass transition temperatures and structural characterization. In addition, the chemical compositions of the annealed glasses were analyzed. The CaO, SiO₂, and Al₂O₃ contents were evaluated using inductively coupled

plasma atomic emission spectroscopy, and the content of K₂O was quantified using atomic absorption spectrometry.

2.3 | Viscosity measurement in high-viscosity region

A parallel plate viscometer (PPVM-1100, OPT Corporation) equipped with an electric resistance furnace (ARF-30KC, ASAHI-RIKA) was newly installed and used to determine the viscosities of the sample melts in the viscosity range of 10⁴–10^{7.5} Pa s. A schematic of the viscometer is shown in Figure 3A. The annealed glass was shaped into cylinders (diameter: 10 mm and height: 5 mm) and sandwiched between two silica glass plates (diameter: 35 mm and thickness: 2 mm). The sample was loaded with a weight of 0.137 kg, and the viscosity was determined by the rate of change in the height of the cylindrical samples, as shown in the following equation³³:

$$\eta' = \frac{2\pi FH^5}{3V \left(\frac{dH}{dt} \right) (2\pi H^3 + V)} \quad (3)$$

where F [N] is the sum of the gravitational force, and V [m³] is the volume of the cylindrical sample with height H [m]. As the relaxation time of the melts is much shorter than 1 s when the melt viscosity is 10⁴–10⁸ Pa s, Fontana³⁴ continuously measured the temperature dependence of the viscosity on the heating process at 10 K/min. Similarly, the present study collected the sample displacement every 30 s, and the viscosity of the sample was evaluated during heating at 4 K/min. The viscosity of a standard glass sample (SRM 717a, National Institute of Standards and Technologies) was measured to calibrate the viscometer. Figure 3B shows the measured viscosity of SRM 717a compared with its recommended values. The difference between the present and recommended values of logarithmic viscosity is approximately 0.21 at the softening points of the SRM 717a ($T = 992 \pm 5$ K, $\log \eta = 6.65$ Pa s). This small difference is due to the inaccuracy of the measured sample temperature. The present study calibrated the measured viscosity η' by the following equation:

$$\text{Log} \eta = 0.21 + \text{Log} \eta' \quad (4)$$

The calibrated viscosity (η) agrees well with the recommended values for the temperature range of 925–1150 K. This calibration methodology was applied to all the samples. Viscosity measurements were performed in the temperature range of 1170–1270 K for the selected calcium aluminosilicate glasses, whereas the examined temperature range was narrower for the K₂O-containing samples to avoid crystallization. To test the reproducibility of

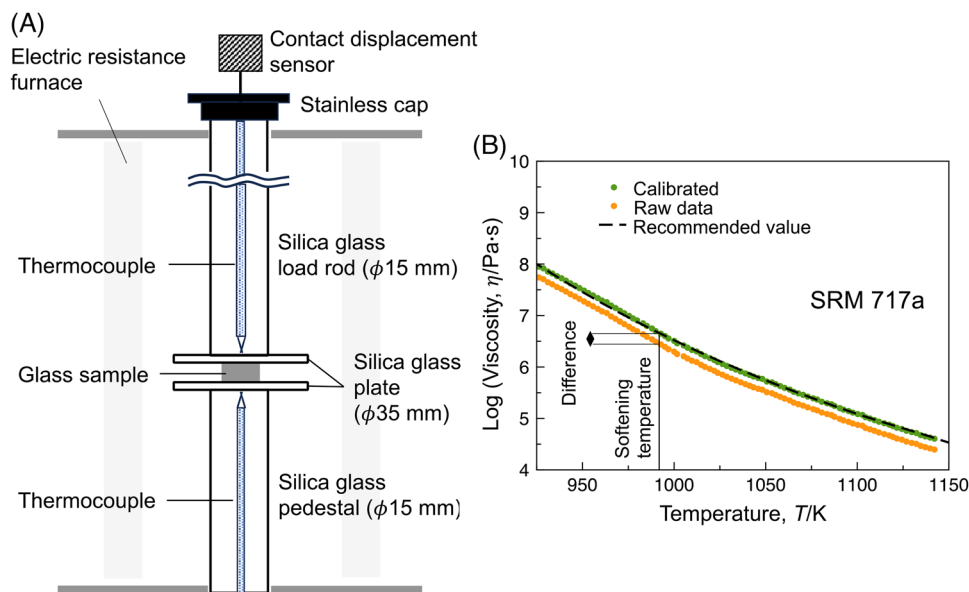


FIGURE 3 (A) Schematics of a parallel plate viscometer used in the present study. The sample temperature is monitored using a thermocouple, which was set above the upper side silica glass plate. A thermocouple set below the lower side silica glass was used to check the temperature homogeneity near the samples. (B) Measured (raw data) and calibrated viscosities of the SRM 717a compared with the recommended values. (Color online).

the measurements, we prepared two pieces of samples for the CAS+7.7K composition and performed viscosity measurements twice. The measured logarithmic viscosity for the two measurements agrees well with $\pm 0.5\%$ scatter.

2.4 | Measurement of T_g

The viscosity of the melt should be close to 10^{12} Pa s at the T_g . The present study evaluated the T_g of the annealed glass samples by DTA using a Thermo Plus Evo TG8120 instrument (RIGAKU Corporation). The annealed glass samples were cylindrical (diameter, 4 mm and height, 1 mm) and placed in a Pt cell (outer diameter, 5 mm and height, 5 mm). The samples were then heated at 10 K/min in air. DTA curves were analyzed to evaluate T_g of the samples.

2.5 | Structural characterizations of the glasses

The local structures of the Al cations were characterized using ^{27}Al magic-angle spinning (MAS) NMR spectroscopy at approximately 300 K using a JNM-ECA 700 spectrometer (JEOL) under a magnetic field of 16.4 T. The powdered sample was packed into a ZrO_2 container and spun at 20 kHz using a JEOL MAS 3.2 mm probe. The NMR signals were measured at a Larmor frequency of

182.4 MHz and collected via single-pulse experiments with a small tip angle ($\pi/10$) and a delay of 5 s. One hundred and twenty-eight scans were performed to obtain each quantitative spectrum,³⁵ and the chemical shifts of the signals were referenced to a 1 M aqueous $\text{Al}(\text{NO}_3)_3$ solution.

Raman spectroscopy is an appropriate technique for characterizing the structures of aluminosilicate anions. Raman spectra of the samples were obtained using a micro-Raman spectrometer (XploRA, Horiba) equipped with a green Ar-ion laser (532 nm). Raman scattering was performed four times with an exposure time of 100 s in the wavenumber range of 25–1500 cm^{-1} , and the intensities of the obtained spectra were normalized relative to their integrated intensities.³⁶ To characterize the detailed compositional dependence of the Raman spectra in the range of 200–1200 cm^{-1} , the effect of the temperature and excitation line on the normalized intensity ($I_{\text{normalized}}$) was corrected by the following equation³⁷:

$$I_{\text{corrected}} = I_{\text{normalized}} \cdot \left\{ \nu_0^3 \cdot \nu \cdot \frac{[1 - \exp(-h\nu/kT)]}{(\nu_0 - \nu)^4} \right\} \quad (5)$$

where h ($= 6.62607 \times 10^{-34}$ J s) is the Planck constant, k ($= 1.38065 \times 10^{-23}$ J K $^{-1}$) is the Boltzmann constant, c ($= 2.9979 \times 10^{10}$ cm s $^{-1}$) is the speed of light, T is the absolute temperature, ν_0 is the wavenumber of the incident laser light (10 7 /532), and ν is the measured wavenumber in cm^{-1} .

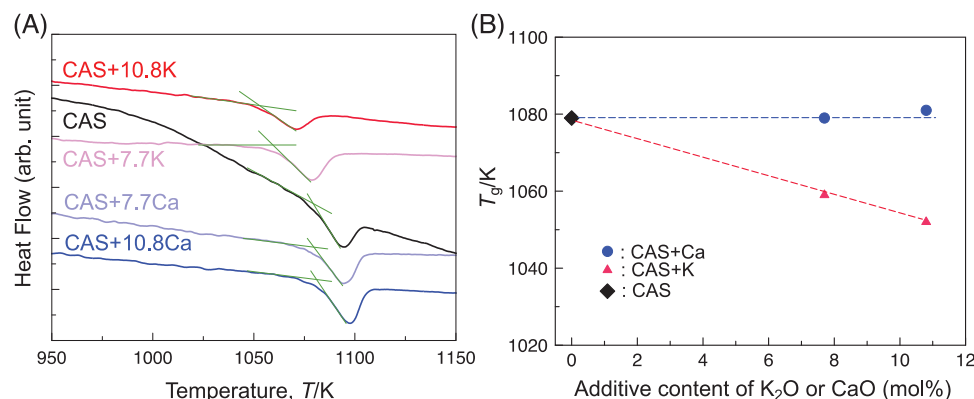


FIGURE 4 (A) Differential thermal analysis (DTA) curves of the glass samples. The green lines indicate lines tangent to the curves before and after the glass transition. Their intersection was evaluated as T_g . (B) T_g variation of the CAS glass with the addition of K_2O or CaO . (Color online).

TABLE 2 Observed T_g by differential thermal analysis (DTA) and fitting parameters for the temperature dependence of the viscosity using Vogel–Fulcher–Tammann (VFT) and MYEGA models.

Samples	T_g/K	VFT parameters			MYEGA parameters	
		A	B	C	m	$\log \eta_\infty$
CAS	1079 ± 2	−3.64	3677	844	52	−1.43
CAS + 7.7K	1059 ± 2	−3.76	4037	803	47	−1.58
CAS + 10.8K	1052 ± 2	−3.89	4280	783	45	−1.71
CAS + 7.7Ca	1079 ± 2	−4.04	3699	849	55	−1.78
CAS + 10.8Ca	1081 ± 2	−4.11	3685	853	56	−1.82

3 | RESULTS AND DISCUSSION

3.1 | Sample composition and glass transition temperature

Table 1 shows the analyzed compositions of the samples after the viscosity measurements in the low-viscosity region. The analyzed compositions agreed well with the nominal values. The present study displays the data using nominal compositions.

Figure 4A shows the DTA curves of the glass samples. The present study defines T_g as the intersection of a line tangent to the curve before the transition begins and another line tangent to the curve immediately after the glass transition.³⁸ The evaluated T_g is plotted in Figure 4B and listed in Table 2. As shown in Figure 4B, T_g of the CAS glass decreased by adding K_2O , whereas T_g of the CAS glass was not sensitive to the addition of CaO . The present study defines the viscosity of the samples as 10^{12} Pa s at the observed T_g by the present DTA measurements.

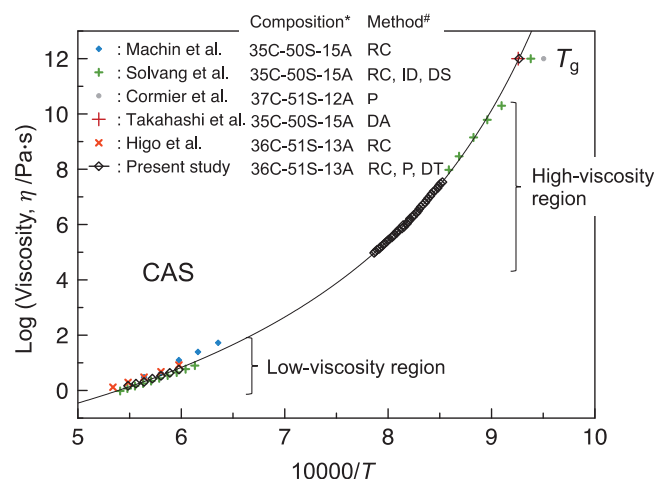


FIGURE 5 Relationship between $\log \eta$ and $10000/T$ for the CAS melt compared with reported values^{26,39–42} for similar compositions. The solid black line displays the fitted Vogel–Fulcher–Tammann (VFT) curve for the present viscosity data for the CAS melt. *C, CaO (mol.%); S, SiO_2 (mol.%); A, Al_2O_3 (mol.%).# DA, dilatometer; DT, DTA; DS, differential scanning calorimetry; ID, indentation method; P, parallel plate method; RC, rotating cylinder method. (Color online).

3.2 | Viscosity and fragility

Figure 5 compares the relationship between the logarithmic viscosity ($\log \eta$) and reciprocal temperature ($1/T$) for the CAS melt with those reported in the literature^{26,39–42} for a similar composition. The viscosity and T_g values of glasses with compositions close to those of CAS have been measured by several researchers. As shown in Figure 5, these reported values have relatively large scatter (e.g., $\pm 40\%$ for the low-viscosity region), which should be because different research groups measure and process the data in different ways, although the principle of

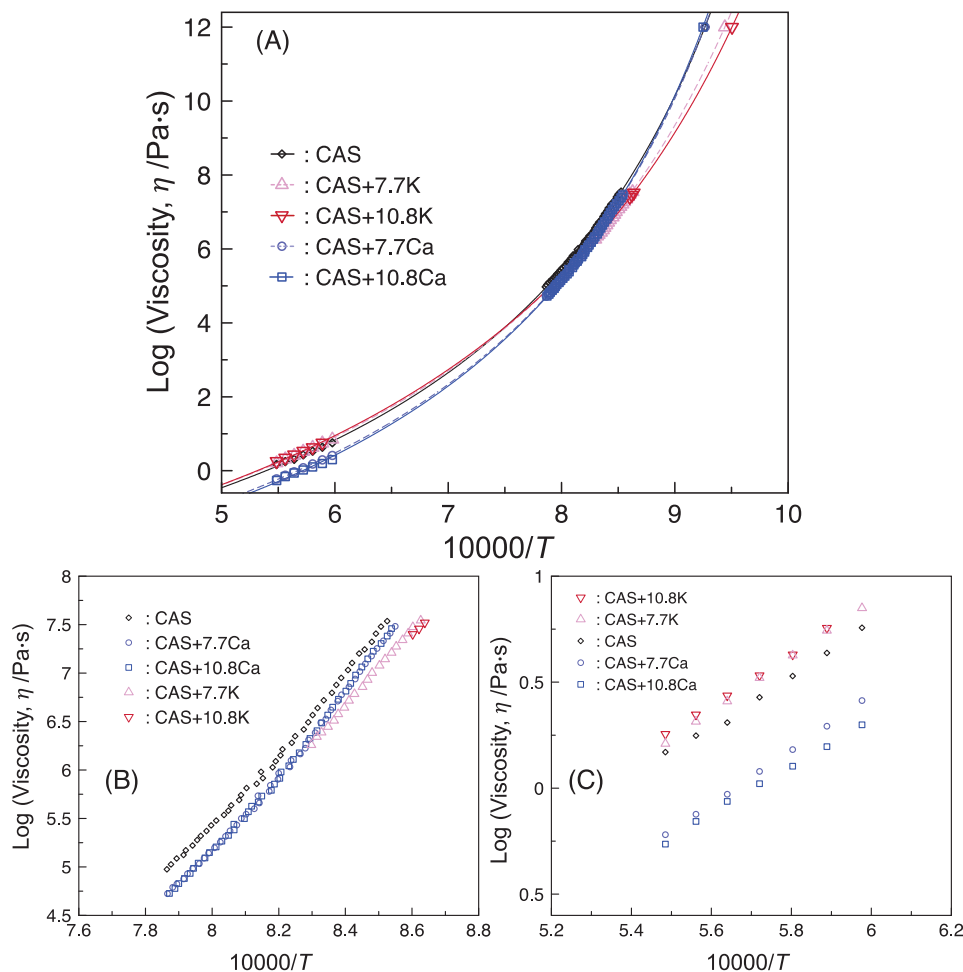


FIGURE 6 (A) Effect of K_2O or CaO addition on the temperature dependence of the viscosity for the CAS melt. The solid and dashed lines indicate fitting curves by the Vogel–Fulcher–Tammann (VFT) model. (B) Viscosity data in the high-viscosity region measured by the parallel plate method. (C) Viscosity data in the low-viscosity region measured by the rotating cylinder method. (Color online).

the measurement is the same. Our viscosity data were plotted in a scattered range, depending on the research group. This verifies the reasonableness of the proposed methodology. Looking at the temperature dependence of the viscosity, the relationship between $\log \eta$ and $1/T$ is not linear. To express viscosity evolution with temperature, the most popular empirical model is as shown in the VFT following equation⁴³:

$$\log \eta = A + \frac{B}{T - C} \quad (6)$$

where A , B , and C are fitting parameters. The variation in viscosity with respect to the temperature was reproduced well by the VFT model (Figure 5).

Figure 6A shows the effect of adding K_2O or CaO on the temperature dependence of the viscosity of the CAS melt. The VFT equation reproduces the temperature dependence. The VFT fitting parameters (A , B , and C) are summarized in Table 2.

As shown in Figure 6B, in the high-viscosity region, the viscosity of the CAS melt decreased with the addition of K_2O or CaO . This tendency indicates that the NBO concentration should dominate the viscosity in the high-viscosity region.

In the low-viscosity region, as shown in Figure 6C, the viscosity of CAS decreases with the addition of CaO , which may be explained by the depolymerization of silicate anions, as indicated by the increase in NBO/T. Conversely, the viscosity of the CAS increases with the addition of K_2O . A similar tendency has been reported in previous studies^{26,44,45} for similar compositions and more complicated systems.^{46–48} However, the underlying mechanism of the viscosity increase in calcium aluminosilicate melts by adding K_2O remains unclear. A possible mechanism for this phenomenon is discussed in Section 4.2.

To evaluate the fragility of the sample melts, $\log \eta$ of the samples is replotted against the T_g -scaled temperature (T_g/T), as shown in Figure 7. Because the present study did not measure the viscosity of the samples at temperatures

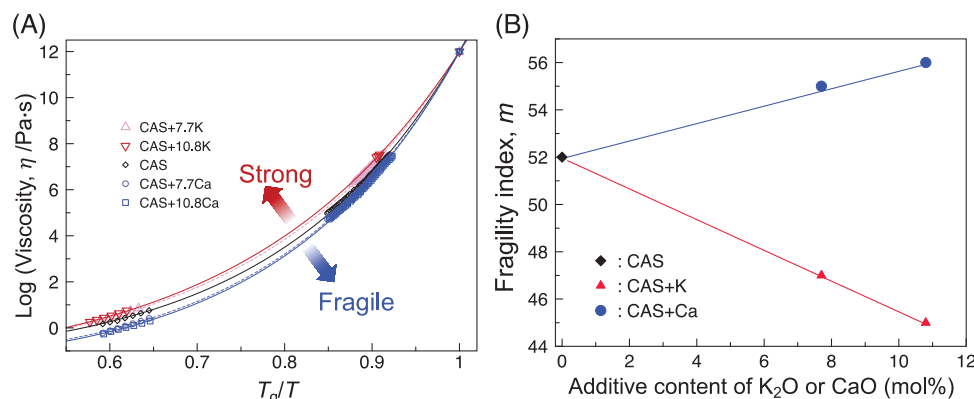


FIGURE 7 (A) $\log \eta$ of the sample glasses is plotted against T_g -scaled temperature (T_g/T). The dashed and solid lines represent the fitting curve obtained the MYEGA model (Equation 7). The red and blue arrows represent the direction of stronger and more fragile behaviors. (B) Effect of the addition of K_2O or CaO on the derived fragility m of the CAS glass. (Color online).

close to the glass transition temperature, it was difficult to derive m by fitting the viscosity data using a linear function (Equation 1). Mauro et al.¹⁰ have developed a viscosity model (the MYEGA model) using m as a fitting parameter:

$$\log \eta = \log \eta_{\infty} + (12 - \log \eta_{\infty}) \cdot \frac{T_g}{T} \cdot \exp \left[\left(\frac{m}{12 - \log \eta_{\infty}} - 1 \right) \left(\frac{T_g}{T} - 1 \right) \right] \quad (7)$$

where $\log \eta_{\infty}$ is an infinite temperature viscosity. The relationship between $\log \eta$ and T_g/T was well fitted by Equation (7). The derived m of CAS, as shown in Table 2 and Figure 7, increases with the addition of CaO , which is consistent with the results of a previous study,⁴⁹ whereas the opposite effect is observed when K_2O is added. CaO and K_2O are common components used to control the physical properties of glasses; however, these additives have contrasting effects on the fragility of the CAS melt.

3.3 | Raman spectroscopy

Figure 8A shows the Raman spectra of the glasses. Aluminosilicate glasses exhibit Raman signals in the boson ($\sim 200 \text{ cm}^{-1}$, ν_1) and low- ($400\text{--}600 \text{ cm}^{-1}$, ν_2 and ν_3), middle- ($600\text{--}800 \text{ cm}^{-1}$, ν_4), and high-wavenumber regions ($800\text{--}1200 \text{ cm}^{-1}$, ν_5).

The Raman signals in the boson region reflect the rotational motions of the almost rigid tetrahedra.⁵⁰ Generally, the peak positions of the boson signals generally shift to higher frequencies with increasing distortion of the TO_4 tetrahedra (T:Si or Al). Figure 8B shows the ν_1 signals of the Raman spectra. The peak position of the ν_1 signal does not change with the addition of CaO , but the signal shifts to a lower frequency when K_2O is added to CAS.

A similar trend was reported when Na was substituted with K in alkali aluminosilicate glasses,⁵⁰ and thus, the levels of distortion of the TO_4 tetrahedra decrease with the addition of K_2O .

To facilitate the comparison of the Raman spectra in the low- and high-wavenumber regions, the temperature and excitation line effect was corrected using Equation (5) and shown in Figure 8C. The Raman signals in the low-wavenumber region are related to the motions of the O atoms in the Si–O–Si linkages, and the peak positions of the signals are associated with the presence of three- to six-membered (or larger) rings. As shown in Figure 8C, two shoulder peaks are observed at approximately $500 (\nu_2)$ and $570 \text{ cm}^{-1} (\nu_3)$ in the Raman spectrum of the CAS glass. The position of the ν_2 signal is close to that of the reported D_1 band (in the spectra of silica and aluminosilicate glasses), indicating the presence of –T–O–T– (T:Si or Al) four-membered rings.⁵¹ The ν_3 signal at 570 cm^{-1} is observed at a slightly different position compared to that of the D_2 band (607 cm^{-1}), which indicates the presence of –Si–O–Si– three-membered rings in a silica glass.⁵¹ However, the peak at $\sim 570 \text{ cm}^{-1}$ is also observed in the spectrum of the $CaAl_2Si_2O_8$ glass and may be assigned to the –T–O–T– three-membered rings in the aluminosilicate glass.⁵² The intensity of ν_2 decreases relative to that of ν_3 by adding K_2O or CaO to the CAS glass. Hence, the relative fraction of four-membered rings decreases with the addition of these non-framework species to the CAS glass, whereas the relative fraction of three-membered rings increases.

Broad, weak signals are observed in the middle-wavenumber regions (ν_4) in the spectra of all samples. This signal is due to the SiO_4 – SiO_4 intertetrahedral linkages,⁵³ but no clear changes based on the composition are observed.

The Raman signal in the high-wavenumber region, which is assigned to the T–O stretching vibration,

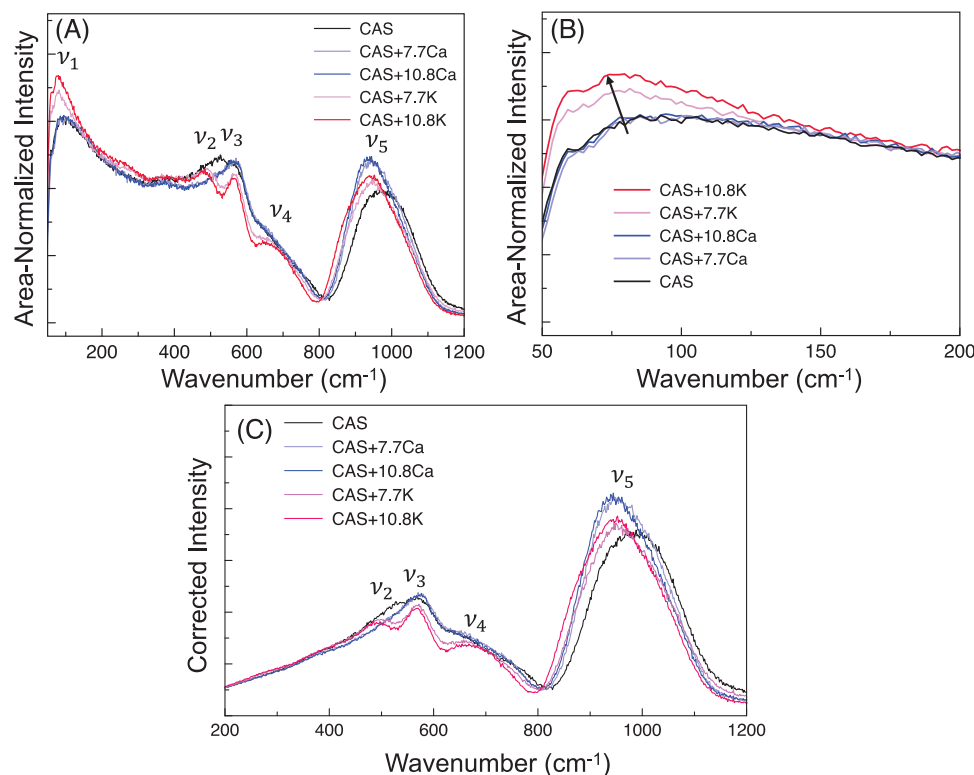


FIGURE 8 (A) Raman spectra of the present aluminosilicate glasses and the (B) magnified spectra in the range 50–200 cm^{-1} . (C) Intensity corrected Raman spectra of the glasses. Temperature and excitation line effects on the area-normalized intensity were corrected using Equation (5). (Color online).

generally shifts to a lower wavenumber with increasing NBO/T and Si substitution with Al. The center of gravity of signal ν_5 shifts to a lower wavenumber upon the addition of K_2O or CaO to the CAS glass, as shown in Figure 8C. Deconvolution of the ν_5 signal is challenging because of the heavy signal overlap. Although it is difficult to experimentally determine the NBO/T values based on Raman spectra, a previous ^{17}O (^{17}O) MAS NMR study²⁶ on $\text{CaO-K}_2\text{O-SiO}_2\text{-Al}_2\text{O}_3$ glass indicated that the experimentally determined NBO/T values are close to the nominal values determined using the compositions. Moreover, the atomic ratio of Al to Si (Al/Si) in the CAS glass increases after the addition of K_2O or CaO , as shown in Table 1. The shift of the ν_5 signal to lower wavenumbers is caused by increases in the NBO/T and Al/Si ratios. Overall, the Raman spectra of the CAS, CAS+K, and CAS+Ca glasses reveal that two types of structural variations occur when K_2O or CaO is added to the CAS glass:

- The levels of distortion of the TO_4 tetrahedra decrease with the addition of K_2O to the CAS glass, whereas the addition of CaO displays little effect on TO_4 distortion.
- The relative fraction of smaller (three-membered) rings increases with the addition of K_2O or CaO .

3.4 | ^{27}Al MAS NMR spectroscopy

Figure 9 shows the ^{27}Al MAS NMR spectra of the glasses. The spectrum of the CAS glass displays a main signal and a small shoulder at ~ 60 and ~ 30 ppm, respectively. The former is assigned to tetrahedrally coordinated Al cations (AlO_4),^{54,55} and the latter indicates the presence of pentacoordinated Al species (AlO_5).^{54,55} The intensity of the signal assigned to AlO_5 decreases with the addition of K_2O to the CAS glass, whereas it does not change significantly with the addition of CaO . The signals representing AlO_4 exhibit asymmetric line shapes with tails toward the low-frequency regions, mainly because of quadrupolar interactions, which may be characterized by the quadrupole coupling constant (C_Q). The linewidth of the CAS glass decreases with the addition of K_2O . The CzSimple model in the DMFIT program (French National Centre for Scientific Research, France)⁵⁶ was used to simulate the line shapes of the signals representing AlO_4 and AlO_5 (Figure S1), and the fitting results are shown in Table 3. The fitting results show that AlO_4 is the major species of aluminum cation in the present glasses. The obtained area fraction of the AlO_5 signal for the annealed CAS glass is approximately 2%, which is slightly lower

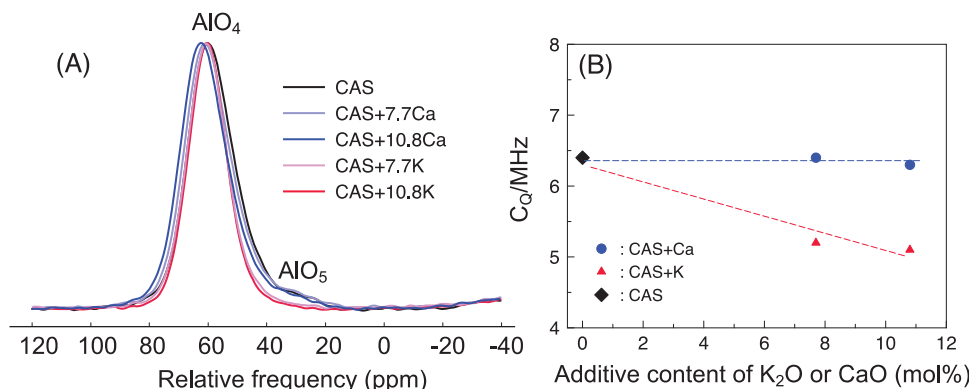


FIGURE 9 (A) ^{27}Al magic-angle spinning (MAS) NMR spectra of the present aluminosilicate glasses and (B) effect of the K_2O or CaO addition on the C_Q of the AlO_4 sites derived from the ^{27}Al MAS NMR spectra. (Color online).

TABLE 3 Fitting parameters of the ^{27}Al magic-angle spinning (MAS) NMR spectra of the present aluminosilicate glasses.

Samples	Area fraction (%)		C_Q (MHz)	
	AlO_4	AlO_5	AlO_4	AlO_5
CAS	98	2	6.4	6.3 ^a
CAS + 7.7K	99	1	5.2	5.2 ^a
CAS + 10.8K	>99.5	<0.5	5.1	5.0 ^a
CAS + 7.7Ca	98	2	6.4	6.3 ^a
CAS + 10.8Ca	98	2	6.3	6.3 ^a

^aFixed parameter.

than that in our previous report³⁵ (~5%) for quenched glass with a similar composition, where the area fraction was obtained by Gaussian fitting. This small difference could be due to the difference in the fitting methodology, as well as the thermal history (i.e., fictive temperature) of the glasses. The area fraction of the minor AlO_5 species is approximately 2% in the CAS- and CaO -added glasses, whereas the K_2O -added CAS glass contains a lower content of AlO_5 species (1%). This tendency may be explained by the smaller Z/N values of the K cations (~0.14) relative to those of the Ca cations (~0.28) because the negative charges of the BOs close to AlO_5 are larger than those of the BOs close to AlO_4 .^{18,19} Overall, the area fractions of AlO_4 in the glasses are >97%, which validates our assumption that the Al cations occur as AlO_4 tetrahedra when calculating the NBO/T of each composition (Table 1). Moreover, the AlO_4 signals of the CAS and CaO -added glasses exhibit larger C_Q values than the AlO_4 signal of the K_2O -added CAS glass (see Figure 9B and Table 3). The C_Q of AlO_4 increases with the shear strain parameter $|\psi|$ of the AlO_4 tetrahedron, as defined by the following equation⁵⁷:

$$|\psi| = \sum_i |\tan(\theta_i - \theta_{\text{ideal}})| \quad (8)$$

The sum is over six O–Al–O bond angles θ_i , and θ_{ideal} is the ideal O–Al–O bond angle (109.5°), as shown in

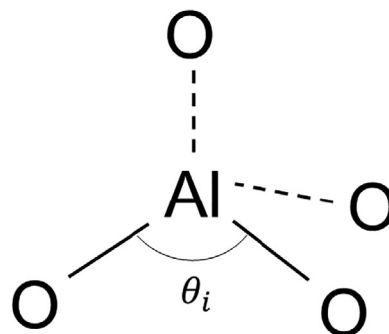


FIGURE 10 Schematic of the structure of an AlO_4 tetrahedron.⁵⁸ θ_i indicates an O–Al–O bond angle.

Figure 10. The derived C_Q values of the glasses indicate that the shear strain (mainly due to the field strengths of the compensator cations) decreases with the addition of K_2O to the CAS glass, whereas the addition of CaO does not significantly affect the shear strain of AlO_4 . This trend is consistent with the variation in the boson peak in the Raman spectrum (Figure 8B).

4 | DISCUSSION

4.1 | Relationship between the fragility and glass structure

Figure 11 schematically shows the possible structures of Ca- and K-doped aluminosilicate glasses. Aluminosilicate glass comprises network structures and weak channels.⁵⁹ The former are generated via the connection of framework cations via BOs with charge compensators, and the latter contains network modifiers and NBOs. The fragility of the melts reflects the structures of both regions. The additive effect of CaO on the fragility of the CAS can be explained by the increased number of weak channels, represented by an increase in NBO/T. Conversely, explaining the decreased

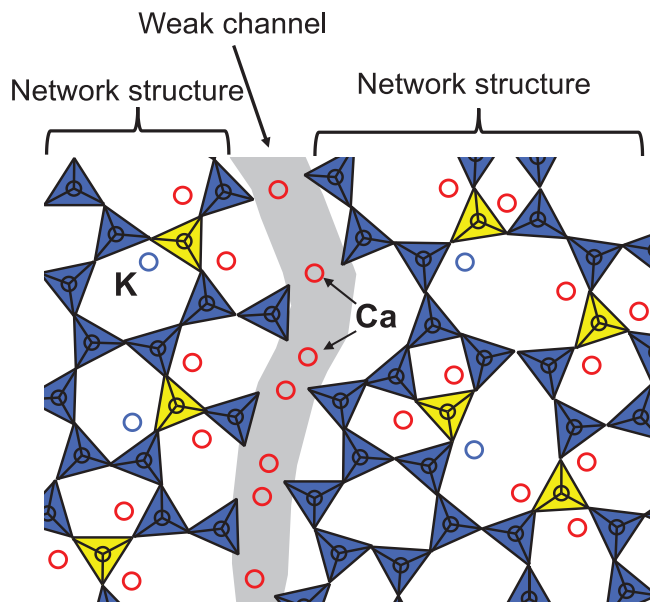


FIGURE 11 Schematic of the in-plane structure of an aluminosilicate glass. The blue and yellow tetrahedra, respectively, represent SiO_4 and AlO_4 . (Color online).

fragility with the addition of K_2O based on NBO/T alone is difficult, and the decrease in fragility should correlate with variations in the network structures. The fragility of the network liquid varies as functions of ring size distribution⁶⁰ and the rigidities of the local structures close to framework cations (e.g., Si^{4+} and Al^{3+}).⁴⁹ Molecular dynamics simulations indicate that large rings (e.g., six-membered rings) are flexible and stress-free, with no internal driving force for structural deformation, whereas smaller rings are relatively strained and thus may exhibit internal stress.⁶⁰ Shi et al.⁶⁰ proposed the average medium-range distance ($\text{MRD}/\text{\AA}$), which is an indicator of ring size distribution. $\text{MRD}/\text{\AA}$ may be calculated using the following equation:

$$\text{MRD}/\text{\AA} = f_{\leq 4 \text{ ring}} \times 3.15 + f_{5 \text{ ring}} \times 3.70 + f_{\geq 6 \text{ ring}} \times 4.30 \quad (9)$$

where $f_{m \text{ ring}}$ is the relative fraction of the m -membered ring, which can be determined from the total neutron scattering of the sample. Although determining the quantitative ring-size distributions (i.e., MRDs) of the samples is challenging, their Raman spectra indirectly indicate that the relative fraction of smaller rings generally increases with the addition of K_2O to the CAS (Figure 8). The variation in the ring size distribution may not explain the decreased fragility due to K_2O addition of, and thus, the rigidities of the local structures close to the Al cations may affect the fragility. Behrens and Schultz⁶¹ proposed that the distortion of the O–T–O bonds (i.e., the shear strain of AlO_4) reduces the energy required to cleave the T–O bond.

The observed C_Q of AlO_4 in the K_2O -added CAS + K indicates that the cleavage and reformation of the Al–O bonds are less pronounced than those in the CAS glass (Table 3). The decrease in the fragility of the CAS with the addition of K_2O is likely due to the decrease in the shear strains of the AlO_4 tetrahedra.

4.2 | Possible mechanism of viscosity increase in CAS by K_2O addition in the low-viscosity region (Hypothesis)

To discuss the viscosity of melts in the low-viscosity region, it is necessary to understand which types of structural characteristics dominate it. The logarithmic viscosity of the aluminosilicate melts decreases nonlinearly with the reciprocal temperature by elevating the temperature of the melts for the wide viscosity range 10^{-1} – 10^{12} Pa s. One of the most successful models for explaining this nonlinear relationship is the Adams–Gibbs (AG) model,⁶² which is represented by the following equation:

$$\log \eta = A_e + \frac{B_e}{T \cdot S_{\text{conf}}(T)} \quad (10)$$

where A_e and B_e are constants, and $S_{\text{conf}}(T)$ is the configurational entropy, which may be determined based on calorimetric data. The AG model assumes the presence of a cooperatively rearranged region (CRR) in the glass structure. When the number of molecules in the CRR is defined as $z(T)$, its relationship with $S_{\text{conf}}(T)$ is represented by the following equation⁶³:

$$z(T) = \frac{s_{\text{conf}}^* \cdot N_A}{S_{\text{conf}}(T)} \quad (11)$$

where s_{conf}^* is the configurational entropy of a single molecule and N_A is Avogadro's number. Because s_{conf}^* is constant depending on the composition and $S_{\text{conf}}(T)$ should increase with increasing temperature, $z(T)$ generally decreases with increasing temperature. Therefore, when the temperature is approximately T_g (i.e., in the high-viscosity region), the variation in the size of the CRR (i.e., $z(T)$) should dominate the temperature dependence of the viscosity. However, in a high-temperature melt with a viscosity close to or lower than 1 Pa s (i.e., the low-viscosity region), the size of the CRR (i.e., $z(T)$) is so small that the average bond strength determines the viscosity.⁶⁴ As K_2O addition decreases the viscosity of silicate melts without alumina in the low-viscosity region,^{65,66} the viscosity (i.e., the average bond strength of the melt) increase in the K_2O -added melts should be related to the interaction between potassium cations and the local structure near aluminum cations. Previous molecular orbital

calculations⁶⁷ for aluminosilicate frameworks indicate that the bond strengths of the Al–O_{BO} and Si–O_{BO} bonds near potassium cations are higher than those near calcium cations in aluminosilicate frameworks, where aluminum cations form AlO₄ tetrahedra. This bond strength variation, depending on the types of nearest non-framework cations (i.e., K⁺ and Ca²⁺), should partially contribute to the viscosity increase in the CAS melt by adding K₂O. However, this contribution will not be the dominant factor in the viscosity increase because the viscosity of molten silicates without alumina does not increase with the addition of K₂O, even if the strength of the Si–O_{BO} bonds increases.

Another aspect of the local structure that can affect the viscosity of aluminosilicate melts is the ordering of the Si and Al cations in the framework. This is known as Löwenstein's rule,⁶⁸ which indicates that the Si–O_{BO}–Al linkage is energetically more favorable than the combination of Si–O_{BO}–Si and Al–O_{BO}–Al species because of the higher negative charge on Al–O_{BO}–Al than on the Si–O_{BO}–Al bridging oxygens. In most cases, Löwenstein's rule is applicable to crystalline aluminosilicate, whereas the rule is partially violated in some aluminosilicate glasses and melts in the peralkaline region.^{69,70} Generally, the strength of T–O_{BO}–T (T = Si or Al) bonds decreases with decreasing bond angle.⁷¹ As the bond angle of Al–O_{BO}–Al is normally narrower than those of the Si–O_{BO}–Si and Si–O_{BO}–Al bonds,⁷¹ the formation of Al–O_{BO}–Al species can decrease the viscosity of aluminosilicate melts in the low-viscosity region. The signal of Al–O_{BO}–Al was undetectable in the previous ¹⁷O NMR spectrum of the CAS glass at room temperature²⁷; however, a non-negligible amount of Al–O_{BO}–Al exists in the molten calcium aluminosilicates at elevated temperatures (e.g., > 1673 K)^{72–74} because its fraction generally increases with increasing temperature. In addition, the amount of Al–O_{BO}–Al depends on the melt composition. Lee and Stebbins⁷² reported that the Al–O_{BO}–Al fraction in calcium aluminosilicate melts was higher than that in alkali aluminosilicate systems. This tendency indicates that the formation of Al–O_{BO}–Al linkages is suppressed by adding K₂O to the CAS melts.

The remaining aspect of the local structure that affects the average bond strength of the melts is the coordination number of the aluminum cations. It is well known that the coordination number of aluminum cations in silicate varies from four to six depending on the composition and temperature, where the field strength (Z/r^2) of aluminum cations increases with a decrease in their coordination number. In glass samples at room temperature, four-coordinated aluminum is the major species (>97%) in the present glass samples. However, an in situ ²⁷Al NMR study⁷⁵ of a 43.1CaO–44.4SiO₂–12.5Al₂O₃ (mol.%) melt indicated the fraction of five-coordinated aluminum cations increases by elevating temperature and should

be close to 20% at 1673 K. In contrast, the formation of five-coordinate aluminum cations was not pronounced for peralkaline sodium aluminosilicate melts.⁵⁰ This indicates that the presence of alkali cations suppresses the increase in the coordination number of aluminum cations in molten aluminosilicates. This is due to the lower bond valence of alkali cations than that of calcium cations, where five-coordinated aluminum cations tend to increase the negative charge on the Si–O_{BO}–Al bridging oxygen.¹⁹ Similarly, the addition of K₂O to the CAS melt should suppress the formation of five-coordinated aluminum cations. Eventually, it is still hypothetical, but the K₂O-induced viscosity increase in the CAS melt in the low-viscosity region can be explained by the reduction of disordered species (i.e., Al–O_{BO}–Al, five-coordinate Al) by adding K₂O to the molten CAS. In situ high-temperature structural characterization⁷⁶ is required to directly prove this hypothesis regarding the mechanism of viscosity increase in the low-viscosity region.

5 | CONCLUSIONS

In this study, the additive effects of K₂O and CaO on the viscosity of a calcium aluminosilicate melt and the obtained data were used to evaluate the fragility of the compositions. The fragility of the calcium aluminosilicate melt increased with the addition of CaO, mainly because of the increased number of nonbridging O atoms. This trend is consistent with the results of a previous study on silicate melts. Conversely, the fragility of the calcium aluminosilicate melt decreased with the addition of K₂O, despite an increase in the number of nonbridging O atoms. This anomalous trend can be explained by the decreased shear strains of the AlO₄ tetrahedra, which increased the resistance of the Al–O bonds to cleavage during melt flow. The addition of an appropriate amount of K₂O to the aluminosilicate melt expanded its working temperature range, facilitating the shaping of the aluminosilicate glass. We also discuss a possible mechanism for the viscosity increase in the CAS melt by adding K₂O to the low-viscosity region. This is still hypothetical; however, the content of disordered species (i.e., Al–O_{BO}–Al, five-coordinate Al), which is undetectable in glass samples at room temperature but non-negligible in the molten state, should dominate the anomalous viscosity increase.

ACKNOWLEDGMENTS

This study was partially supported by the Institute of Multidisciplinary Research for Advanced Materials Project (2014–2015, 2023), JSPS KAKENHI Grant Number JP21H01854, and the Dynamic Alliance for Open Innovation Bridging Human, Environment, and Materials of

the Ministry of Education, Culture, Sports, Science, and Technology of Japan. We thank Mr. Ryo Uchida (Tohoku University) for the sample synthesis. We thank two anonymous reviewers and the editor for their constructive comments on improving our manuscript.

ORCID

Sohei Sukenaga  <https://orcid.org/0000-0002-9086-2784>

Yann Gueguen  <https://orcid.org/0000-0001-6348-3060>

REFERENCES

- Martlew D. Viscosity of molten glass. In: Pye LD, Montenero A, Joseph I, editors. *Properties of glass-forming melts*. Boca Raton, FL: CRC Press; 2005. p. 75–86.
- Avramov I. Viscosity activation energy. *Phys Chem Glasses*. 2007;48:61–63.
- Avramov I. Viscosity in disordered media. *J Non-Cryst Solids*. 2005;351(40–42):3163–73. <https://doi.org/10.1016/j.jnoncrsol.2005.08.021>
- Richet P, Bottinga Y. Rheology and configurational entropy of silicate melts. In: Stebbins JF, McMillan PF, Dingwell DB, editors. *Structure, dynamics and properties of silicate melts*. Chelsea: Mineralogical Society of America; 1995. p. 67–93.
- Angell CA. Formation of glasses from liquids and biopolymers. *Science*. 1995;267(5206):1924–35. <https://doi.org/10.1126/science.267.5206.1924>
- Angell CA. Relaxation in liquids, polymers and plastic crystals—strong/fragile patterns and problems. *J Non-Cryst Solids*. 1991;131–133:13–31. [https://doi.org/10.1016/0022-3093\(91\)90266-9](https://doi.org/10.1016/0022-3093(91)90266-9)
- Smedskjaer MM, Mauro JC, Yue Y. Ionic diffusion and the topological origin of fragility in silicate glasses. *J Chem Phys*. 2009;131(24):244514. <https://doi.org/10.1063/1.3276285>
- Deubener J, Behrens H, Müller R, Zietka S, Reinsch S. Kinetic fragility of hydrous soda-lime-silica glasses. *J Non-Cryst Solids*. 2008;354(42–44):4713–18. <https://doi.org/10.1016/j.jnoncrsol.2008.04.021>
- Karlsson S. Viscosity of alumina doped soda lime silicate glasses—observation of anomaly in the linear increase as Al_2O_3 replaces SiO_2 . *J Non-Cryst Solids*. 2021;573:121149. <https://doi.org/10.1016/j.jnoncrsol.2021.121149>
- Mauro JC, Yue Y, Ellison AJ, Gupta PK, Allan DC. Viscosity of glass-forming liquids. *Proc Natl Acad Sci USA*. 2009;106(47):19780–84. <https://doi.org/10.1073/pnas.0911705106>
- Wilding MC, Delaizir G, Benmore CJ, Gueguen Y, Dolhen M, Duclère JR, et al. Structural studies of Bi_2O_3 – Nb_2O_5 – TeO_2 glasses. *J Non-Cryst Solids*. 2016;451:68–76. <https://doi.org/10.1016/j.jnoncrsol.2016.07.004>
- Wang J, Wu M, Tang H, Han J, Liu C, Cao X, et al. Correlation between viscosity, electrical resistivity and network connectivity of alkali-free boroaluminosilicate glasses *J Non-Cryst Solids*. 2019;509:88–94. <https://doi.org/10.1016/j.jnoncrsol.2018.12.037>
- Cheng J, Xiao Z, Yang K, Wu H. Viscosity, fragility and structure of Na_2O – CaO – Al_2O_3 – SiO_2 glasses of increasing Al/Si ratio. *Ceram Int*. 2013;39(4):4055–62. <https://doi.org/10.1016/j.ceramint.2012.10.258>
- Poole JP. Low-temperature viscosity of alkali silicate glasses. *J Am Ceram Soc*. 1949;32(7):230–33. <https://doi.org/10.1111/j.1151-2916.1949.tb18952.x>
- Sidebottom DL. The fragility of alkali silicate glass melts: part of a universal topological pattern. *J Non-Cryst Solids*. 2019;516:63–66. <https://doi.org/10.1016/j.jnoncrsol.2019.04.033>
- Giordano D, Dingwell DB. The kinetic fragility of natural silicate melts. *J Phys: Condens Matter*. 2003;15(11):S945–54. <https://doi.org/10.1088/0953-8984/15/11/318>
- Nascimento MLF, Aparicio C. Viscosity of strong and fragile glass-forming liquids investigated by means of principal component analysis. *J Phys Chem Solids*. 2007;68:104–10. <https://doi.org/10.1016/j.jpcs.2006.09.013>
- Stebbins JF, Wu J, Thompson LM. Interactions between network cation coordination and non-bridging oxygen abundance in oxide glasses and melts: insights from NMR spectroscopy. *Chem Geol*. 2013;346:34–46. <https://doi.org/10.1016/j.chemgeo.2012.09.021>
- Sukenaga S, Kanehashi K, Yamada H, Ohara K, Wakiyama T, Shibata H. Mechanism of Al coordination change in alkaline-earth aluminosilicate glasses: an application of bond valence model. *ISIJ Int*. 2023;63:1263–66. <https://doi.org/10.2355/isijinternational.ISIJINT-2022-398>
- Mysen B. Structure of aluminosilicate melts. *ISIJ Int*. 2021;61(12):2866–81. <https://doi.org/10.2355/isijinternational.ISIJINT-2021-100>
- Brwon ID. *The chemical bond in inorganic chemistry, the bond valence model*. Oxford: Oxford University Press; 2016.
- Sukenaga S, Florian P, Kanehashi K, Shibata H, Saito N, Nakashima K, et al. Oxygen speciation in multicomponent silicate glasses using through bond double resonance NMR spectroscopy. *J Phys Chem Lett*. 2017;8(10):2274–79. <https://doi.org/10.1021/acs.jpclett.7b00465>
- Cormier L, Neuville DR. Ca and Na environments in Na_2O – CaO – Al_2O_3 – SiO_2 glasses: influence of cation mixing and cation-network interactions. *Chem Geol*. 2004;213(1–3):103–13. <https://doi.org/10.1016/j.chemgeo.2004.08.049>
- Waseda Y, Suito H. The structure of molten alkali metal silicates. *Trans Iron Steel Inst Jpn*. 1977;17(2):82–91. <https://doi.org/10.2355/isijinternational1966.17.82>
- Shimoda K, Tobu Y, Shimoikeda Y, Nemoto T, Saito K. Multiple Ca^{2+} environments in silicate glasses by high-resolution ^{43}Ca MQMAS NMR technique at high and ultra-high (21.8T) magnetic fields. *J Magn Reson*. 2007;186(1):156–59. <https://doi.org/10.1016/j.jmr.2007.01.019>
- Higo T, Sukenaga S, Kanehashi K, Shibata H, Osugi T, Saito N, et al. Effect of potassium oxide addition on viscosity of calcium aluminosilicate melts at 1673–1873 K. *ISIJ Int*. 2014;54(9):2039–44. <https://doi.org/10.2355/isijinternational.54.2039>
- Sukenaga S, Kanehashi K, Shibata H, Saito N, Nakashima K. Structural role of alkali cations in calcium aluminosilicate glasses as examined using oxygen-17 solid-state nuclear magnetic resonance spectroscopy. *Metall Mater Trans B*. 2016;47(4):2177–81. <https://doi.org/10.1007/s11663-016-0689-7>
- Toplis MJ, Dingwell DB, Hess KU, Lenci T. Viscosity, fragility, and configurational entropy of melts along the join SiO_2 – NaAlSiO_4 . *Am Mineral*. 1997;82(9–10):979–90. <https://doi.org/10.2138/am-1997-9-1014>

29. Bechgaard TK, Mauro JC, Bauchy M, Yue Y, Lamberson LA, Jensen LR, et al. Fragility and configurational heat capacity of calcium aluminosilicate glass-forming liquids. *J Non-Cryst Solids*. 2017;461:24–34. <https://doi.org/10.1016/j.jnoncrsol.2017.01.033>
30. Mysen B, Richet P. Melt and glass structure. In: Mysen B, Richet P, editors. *Silicate glasses and melts*. Amsterdam: Elsevier; 2005. p. 101–29.
31. Sukenaga S, Shibata H. High-temperature characterization of glasses and melts. In: Pomeroy M, editor. *Encyclopedia of materials: technical ceramics and glasses*. Oxford: Elsevier; 2021. p. 689–703. <https://doi.org/10.1016/B978-0-12-818542-1.00024-2>
32. Sukenaga S, Ogawa M, Yanaba Y, Ando M, Shibata H. Viscosity of Na–Si–O–N–F melts: mixing effect of oxygen, nitrogen, and fluorine. *ISIJ Int*. 2020;60(12):2794–806. <https://doi.org/10.2355/isijinternational.2020-326>
33. Gent AN. Theory of the parallel plate viscometer. *Br J Appl Phys*. 1960;11:85–87. <https://doi.org/10.1088/0508-3443/11/2/310>
34. Fontana EH. A versatile parallel-plate viscometer for glass viscosity measurements to 1000°C. *Am Ceram Soc Bull*. 1970;49(6):594.
35. Sukenaga S, Nagahisa T, Kanehashi K, Saito N, Nakashima K. Reconsideration on Al coordination in CaO–SiO₂–Al₂O₃–(R₂O or RO) glasses by using high field solid-state ²⁷Al NMR spectroscopy. *ISIJ Int*. 2011;51(2):333–35. <https://doi.org/10.2355/isijinternational.51.333>
36. Sukenaga S, Unozawa H, Chiba Y, Tashiro M, Kawanishi S, Shibata H. Incorporation limit of MoO₃ in sodium borosilicate glasses. *J Am Ceram Soc*. 2023;106(1):293–305. <https://doi.org/10.1111/jace.18760>
37. Neuville DR, De Ligny D, Henderson GS. Advances in Raman spectroscopy applied to earth and material sciences. In: Henderson GS, Neuville DR, Downs RT, editors. *Spectroscopic methods in mineralogy and materials sciences*. Volume 78, Reviews in mineralogy and geochemistry. Chantilly: Mineralogical Association of America; 2014. p. 509–41. <https://dx.doi.org/10.2138/rmg.2013.78.13>
38. Koontz E. Thermal analysis of glass. In: Musgraves JD, Hu J, Calvez L, editors. *Springer handbook of glass*. Cham: Springer Nature; 2019. p. 853–78. https://doi.org/10.1007/978-3-319-93728-1_24
39. Machin JS, Yee TB. Viscosity studies of system CaO–MgO–Al₂O₃–SiO₂: II, CaO–Al₂O₃–SiO₂. *J Am Ceram Soc*. 1948;31(7):200–204. <https://doi.org/10.1111/j.1151-2916.1948.tb14290.x>
40. Solvang M, Yue YZ, Jensen SL, Dingwell DB. Rheological and thermodynamic behaviors of different calcium aluminosilicate melts with the same non-bridging oxygen content. *J Non-Cryst Solids*. 2004;336:179–88. <https://doi.org/10.1016/j.jnoncrsol.2004.02.009>
41. Cormier L, Neuville DR, Calas G. Relationship between structure and glass transition temperature in low-silica calcium aluminosilicate glasses: the origin of the anomaly at low silica content. *J Am Ceram Soc*. 2005;88(8):2292–99. <https://doi.org/10.1111/j.1551-2916.2005.00428.x>
42. Takahashi S, Ueda K, Saitoh A, Takebe H. Compositional dependence of the thermal properties and structure of CaO–Al₂O₃–SiO₂ glasses with a molar ratio of CaO/Al₂O₃>1. *J MMIJ*. 2012;128(3):150–54. <https://doi.org/10.2473/journalofmmij.128.150>
43. Fulcher GS. Analysis of recent measurements of the viscosity of glasses. *J Am Ceram Soc*. 1925;8(6):339–55. <https://doi.org/10.1111/j.1151-2916.1925.tb16731.x>
44. Sukenaga S, Saito N, Kawakami K, Nakashima K. Viscosities of CaO–SiO₂–Al₂O₃–(R₂O or RO) melts. *ISIJ Int*. 2006;46(3):352–58. <https://doi.org/10.2355/isijinternational.46.352>
45. Zhang G-H, Chou K-C. Measuring and modeling viscosity of CaO–Al₂O₃–SiO₂–(K₂O) melt. *Metall Mater Trans B*. 2012;43:841–48. <https://doi.org/10.1007/s11663-012-9668-9>
46. Kim WH, Sohn I, Min DJ. A study on the viscous behavior with K₂O additions in the CaO–SiO₂–Al₂O₃–MgO–K₂O quinary slag system. *Steel Res Int*. 2010;81(9):735–41. <https://doi.org/10.1002/srin.201000067>
47. Chang Z-Y, Jiao K-X, Ning X-J, Zhang J-L. Novel approach to studying influences of Na₂O and K₂O additions on viscosity and thermodynamic properties of BF slags. *Metall Mater Trans B*. 2019;50:1399–406. <https://doi.org/10.1007/s11663-019-01565-5>
48. Liu W, Xing X, Zuo H. The viscous behavior and potassium removal capacity of CaO–SiO₂–8wt%MgO–17wt%Al₂O₃–2.5wt%BaO–K₂O slag. *Metall Res Technol*. 2020;117(2):201. <https://doi.org/10.1051/metal/2020013>
49. Moesgaard M, Yue Y. Compositional dependence of fragility and glass forming ability of calcium aluminosilicate melts. *J Non-Cryst Solids*. 2009;355(14–15):867–73. <https://doi.org/10.1016/j.jnoncrsol.2009.04.004>
50. Le Losq C, Neuville DR. Effect of the Na/K mixing on the structure and the rheology of tectosilicate silica-rich melts. *Chem Geol*. 2013;346:57–71. <https://doi.org/10.1016/j.chemgeo.2012.09.009>
51. Galeener FL. Planar rings in vitreous silica. *J Non-Cryst Solids*. 1982;49:53–62. [https://doi.org/10.1016/0022-3093\(82\)90108-9](https://doi.org/10.1016/0022-3093(82)90108-9)
52. Sharma SK, Philpotts JA, Matson DW. Ring distributions in alkali- and alkaline-earth aluminosilicate framework glasses—a Raman spectroscopic study. *J Non-Cryst Solids*. 1985;71(1–3):403–10. [https://doi.org/10.1016/0022-3093\(85\)90311-4](https://doi.org/10.1016/0022-3093(85)90311-4)
53. Bechgaard TK, Scannell G, Huang L, Youngman RE, Mauro JC, Smedskjaer MM. Structure of MgO/CaO sodium aluminosilicate glasses: Raman spectroscopy study. *J Non-Cryst Solids*. 2017;470:145–51. <https://doi.org/10.1016/j.jnoncrsol.2017.05.014>
54. Novikov AN, Neuville DR, Hennet L, Gueguen Y, Thiaudière D, Charpentier T, et al. Al and Sr environment in tectosilicate glasses and melts: viscosity, Raman and NMR investigation. *Chem Geol*. 2017;461:115–27. <https://doi.org/10.1016/j.chemgeo.2016.11.023>
55. Iftekhhar S, Pahari B, Okhotnikov K, Jaworski A, Svensson B, Grins J, et al. Properties and structures of RE₂O₃–Al₂O₃–SiO₂ (RE = Y, Lu) glasses probed by molecular dynamics simulations and solid-state NMR: the roles of aluminum and rare-earth ions for dictating the microhardness. *J Phys Chem C*. 2012;116(34):18394–406. <https://doi.org/10.1021/jp302672b>
56. Massiot DM, Fayon F, Capron M, King I, Le Calvé S, Alonso B, et al. Modelling one and two dimensional solid state NMR spectra. *Magn Reson Chem*. 2002;40(1):70–76. <https://doi.org/10.1002/mrc.984>
57. Ghose S, Tsang T. Structural dependence of quadrupole coupling constant e²qQ/h for ²⁷Al and crystal field parameter D for Fe³⁺ in aluminosilicates. *Am Mineral*. 1973;58(7–8):748–55

58. Sukenaga S, Ikoma R, Tashiro M, Chiba Y, Kawanishi S, Shibata H. $\text{AlO}_{1.5}/\text{SiO}_2$ substitution effect on the viscosity of alkali silicate melts. *High Temp—High Pressures*. 2023;52(3–4):195–210. <https://doi.org/10.32908/hthp.v5.1437>
59. Greaves GN. EXAFS and the structure of glass. *J Non-Cryst Solids*. 1985;71(1–3):203–17. [https://doi.org/10.1016/0022-3093\(85\)90289-3](https://doi.org/10.1016/0022-3093(85)90289-3)
60. Shi Y, Deng B, Gulbitten O, Bauchy M, Zhou Q, Neufeind J, et al. Revealing the relationship between liquid fragility and medium-range order in silicate glasses. *Nat Commun*. 2023;14(1):13. <https://doi.org/10.1038/s41467-022-35711-6>
61. Behrens H, Schulze F. Pressure dependence of melt viscosity in the system $\text{NaAlSi}_3\text{O}_8$ – $\text{CaMgSi}_2\text{O}_6$. *Am Mineral*. 2004;88(8–9):1351–63. <https://doi.org/10.2138/am-2003-8-919>
62. Adam G, Gibbs JH. On the temperature dependence of cooperative relaxation properties in glass-forming liquids. *J Chem Phys*. 1965;43:139–46. <https://doi.org/10.1063/1.1696442>
63. Yamamuro O, Tsukushi I, Lindqvist A, Takahara S, Ishikawa M, Matsuo T. Calorimetric study of glassy and liquid toluene and ethylbenzene: thermodynamic approach to spatial heterogeneity in glass-forming molecular liquids. *J Phys Chem B*. 1998;102:1605–9. <https://doi.org/10.1021/jp973439v>
64. Toplis MJ, Dingwell DB. Shear viscosities of CaO – Al_2O_3 – SiO_2 and MgO – Al_2O_3 – SiO_2 liquids: implications for the structural role of aluminum and degree of polymerization of synthetic and natural aluminosilicate melts. *Geochim Cosmochim Acta*. 2004;68:5169–88. <https://doi.org/10.1016/j.gca.2004.05.041>
65. Bockris JO'M, Mackenzie JD, Kitchner JA. Viscous flow in silica and binary liquid silicates. *Trans Faraday Soc*. 1955;51:1734–48. <https://doi.org/10.1039/TF9555101734>
66. Yasukouchi T, Nakashima K, Mori K. Viscosity of ternary CaO – SiO_2 – $\text{M}_x(\text{F},\text{O})_y$ and CaO – Al_2O_3 – Fe_2O_3 melts. *Tetsu-to-Hagane*. 1999;85(8):571–77. https://doi.org/10.2355/tetsutohagane1955.85.8_571
67. Geisinger KL, Gibbs GV, Navrotsky A. A molecular orbital study of bond length and angle variations in framework structures. *Phys Chem Mineral*. 1985;11:266–83. <https://doi.org/10.1007/BF00307405>
68. Loewenstein W. The distribution of aluminum in the tetrahedra of silicates and aluminates. *Am Mineral*. 1954;39(1–2):92–96
69. Lee SK, Stebbins JF. Disorder and the extent of polymerization in calcium silicate and aluminosilicate glasses: O-17 NMR results and quantum chemical molecular orbital calculations. *Geochim Cosmochim Acta*. 2006;70(16):4275–86. <https://doi.org/10.1016/j.gca.2006.06.1550>
70. Lee SK, Kim H-I, Kim EJ, Mun KY, Ryu S. Extent of disorder in magnesium aluminosilicate glasses: insights from ^{27}Al and ^{17}O NMR. *J Phys Chem C*. 2016;120(1):737–49. <https://doi.org/10.1021/acs.jpcc.5b10799>
71. Navrotsky A, Geisinger KL, McMillan P, Gibbs GV. The tetrahedral framework in glasses and melts? Inferences from molecular orbital calculations and implications for structure, thermodynamics, and physical properties. *Phys Chem Minerals*. 1985;11:284–98. <https://doi.org/10.1007/BF00307406>
72. Lee SK, Stebbins JF. Al–O–Al and Si–O–Si sites in framework aluminosilicate glasses with Si/Al = 1: quantification of framework disorder. *J Non-Cryst Solids*. 2000;270(1–3):260–64. [https://doi.org/10.1016/S0022-3093\(00\)00089-2](https://doi.org/10.1016/S0022-3093(00)00089-2)
73. Stebbins JF. Temperature effects on the network structure of oxide melts and their consequences for configurational heat capacity. *Chem Geol*. 2008;256:80–91. <https://doi.org/10.1016/j.chemgeo.2008.03.011>
74. Greenberg B, Garofalini SH. Molecular simulations of the structure and thermal transport of high alumina aluminosilicate molten core glass fiber. *J Am Ceram Soc*. 2018;101(7):2941–50. <https://doi.org/10.1111/jace.15471>
75. Stebbins JF, Dubinsky EV, Kanehashi K, Kelsey KE. Temperature effects on non-bridging oxygen and aluminum coordination number in calcium aluminosilicate glasses and melts. *Geochim Cosmochim Acta*. 2008;72(3):910–25. <https://doi.org/10.1016/j.gca.2007.11.018>
76. Florian P, Novilov A, Drewitt JW, Hennem L, Sarou-Kanian V, Massiot D, et al. Structure and dynamics of high-temperature strontium aluminosilicate melts. *Phys Chem Chem Phys*. 2018;20:27865–77. <https://doi.org/10.1039/C8CP04908D>

SUPPORTING INFORMATION

Additional supporting information can be found online in the Supporting Information section at the end of this article.

How to cite this article: Sukenaga S, Gueguen Y, Celarie F, Rouxel T, Tashiro M, Yoshida S, et al. Effect of calcium and potassium oxide addition on the viscosity and fragility of a calcium aluminosilicate melt. *J Am Ceram Soc*. 2024;107:3822–36. <https://doi.org/10.1111/jace.19722>